www.RedMountainRadio.com

Thanks for your interest in my technical paper. If you find this work to be interesting, or have additional questions, please contact me at the address below. Red Mountain Radio LLC offers professional RF, optical, and microwave design services, and problem solving.

Regards,
Eric Funk, Ph. D.
Partner, Red Mountain Radio LLC
eric@redmountainradio.com
970-325-2158 ×12

Free-Space Power Combining and Beam Steering of Ultra-Wideband Radiation Using an Array of Laser-Triggered Antennas

Eric E. Funk and Chi H. Lee

Abstract— **A mode-locked laser is used to synchronize jitter-free ultrawideband (UWB) pulse generation at an array of UWB antenna elements. The jitter-free pulses radiated by each element add together in free space to produce a radiated field pattern that is steerable via optical true-time-delay techniques. The results from a three element array experiment are presented and used to develop a model for an N-element phased array. A transmission-line model is presented for a single array element, which includes the functions of energy storage, as well as UWB pulse generation and radiation.**

I. Introduction

A VARIETY of approaches to photonic control of microwave phased-array antenna systems have received much interest lately. The goal is to replace bulky electrical feed lines with lightweight optical fibers. The conventional approach [1], [2] involves modulating a continuous wave (CW) laser with narrowband RF, coupling the optical signal into a fiber, and converting back to an RF signal at each antenna element with a photodiode. Thus, the RF signal suffers from dynamic range limitations resulting from laser noise, electrical-to-optical insertion losses, and distortion caused by nonlinearities in modulation.

Our approach circumvents the usual electrical to optical conversion loss by using a laser to deliver synchronization pulses rather than the RF signal. Optical trigger pulses from a mode-locked laser trigger the generation of ultra-wideband (UWB) RF at each of the antenna elements, as shown in Fig. 1. When the elements are triggered simultaneously, the electric fields from each of the individual elements combine coherently in free space at an angle $\phi_0 = 0°$. Hence, the peak power received by a far-field antenna placed at $0°$ scales as N^2, where N is the number of radiating elements. Furthermore, one can steer the beam of UWB radiation from $\phi = 0°$ to $\phi = 90°$ by adjusting the arrival time of the optical pulses that trigger the individual elements; this optical control technique is a form of true time delay [1]–[5].

Unlike many conventional optically controlled phased arrays, our phased array radiates instantaneously UWB RF.

Manuscript received October 3, 1995; revised July 22, 1996. This work was supported in part by The High-Power Microwave Technology Office at the Army Research Laboratory.

E. E. Funk is with the Army Research Laboratory, Weapons Technology Directorate, Adelphi, MD 20783 USA.

C. H. Lee is with the University of Maryland, Department of Electrical Engineering, College Park, MD 20742 USA.

Publisher Item Identifier S 0018-9480(96)07911-2.

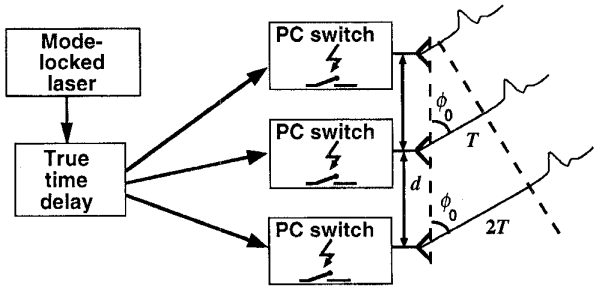

Fig. 1. System architecture employing true time delay (TTD). TTD gives a relative delay of T between adjacent elements, causing UWB beam to be steered at an angle of ϕ_0.

The synchronized UWB signal may be useful in a variety of applications, but perhaps the most interesting potential use is in the development of communications links. The exceptionally large bandwidth that is available will allow the design of spread-spectrum communications systems with extremely high processing gains [6], [7].

In this paper, we present a demonstration of this technique using an Si photoconductor as a jitter-free closing switch [8] to trigger UWB pulse generation [9] at three passive bow-tie antenna [10] elements. We first present an analysis of a single laser-triggered bow-tie antenna element. We show how this element effectively combines the tasks of capacitive energy storage, pulse generation, and radiation [11]. We then present an experimental demonstration of the coherent addition of UWB pulsed radiation in free space from three laser triggered antenna elements. We also present a demonstration of UWB beam steering using optical true time delay (TTD). The results from the three-element experiment are then used in a computational model to predict the results that we would expect from a larger (N-element) array. Since our antenna elements were *not* driven by CW signals, but rather by pulsed signals, we have focused on a time-domain analysis.

We note that in the past, similar photoconductive switching techniques have been used for the generation of ultra-short electrical pulses with millimeter wavelengths [12]–[14]. The millimeter wavelength radiation is useful for specialized applications, including millimeter-wave spectroscopy [15]. However, the propagation distance of the millimeter-wave signal is usually quite limited, and opto-electronic sampling techniques are usually required for reception. Hence, we sought to de-

velop a longer wavelength system that was more appropriate for phased-array radar or a spread-spectrum communications link, where propagation distances are large and all-electronic receivers may be used.

II. Experimental Setup and Model Verification

The three elements of our laser-triggered array are shown in Fig. 2. An element consists of a bow-tie antenna of length $b = 5.7$ cm and angle $\beta = 27°$. The bowtie elements were patterned photographically on a thin (0.008-in) coating of copper on one side of a 1/16-in thick glass-epoxy circuit board. The other side of the board was uncoated (i.e., no ground plane was used). In order to avoid dispersive effects, the thickness of the circuit board was chosen to be a small fraction of a wavelength even at the highest frequencies radiated. An Si photoconductor, with a lateral 1-mm gap size and aluminum contacts, was electrically connected to the apex of the top and bottom halves of the antenna in order to provide an optically triggered transient. With this geometry, the photoconductor had a 47-pF capacitance at 1 kHz. The bottom and top halves of each antenna were pulse charged with opposite polarity to $\pm V_0 = 410$ V through a 1-kΩ discrete 1/4-W resistor and in synchronization with a 540-Hz optical pulse train, which was focused onto the gap of each photoconductor. The photoconductor produced a fast risetime (<1 ns into 50 Ω) and slow fall-time (on the order of microseconds), step-like electrical pulse when triggered with our laser pulse. The optical system consisted of a compact, diode-laser pumped, mode-locked Nd : YLF laser and regenerative amplifier. The regenerative amplifier delivered a 540-Hz train of 5-mJ, 126-ps full width at half maximum, pulses at a wavelength of 1.053 μm. The optical pulse-to-pulse jitter of the laser was better than our sampling oscilloscope measurement limit of 4 ps.

Before the photoconductors were installed on the bow-tie antennas, we characterized one of the antennas by time-domain reflectometry (TDR) measurements [16] in order to verify our transmission-line energy storage model. The TDR measurement was made with a Tektronix 11 802 sampling oscilloscope, which fed the bow-tie antenna with a step function excitation through a 50-Ω transmission line.

Three of the laser-triggered UWB bow-tie antenna elements were then assembled together into an array. Fig. 2 shows a detailed view of the array and the orientation of the elements with respect to the UWB field sensor. The laser beam used to trigger the antennas was split into three beams via the use of half-wave plates and polarizing beam splitters. The optical beam path to two of the three elements included an adjustable time delay using prisms mounted on precision translation stages. Each of the three laser beams was then focused onto the photoconductive gap of a corresponding photoconductor. An electrically short conical monopole antenna (CMA) field probe antenna with $a = 1.3$ cm and $\alpha = 47°$ (see Fig. 2) was placed 1 m from the plane of the array at the azimuth angle ϕ and an elevation angle of 0°. The short CMA field probe sensed the derivative of the incident field when fed into a matched 50-Ω load [17].

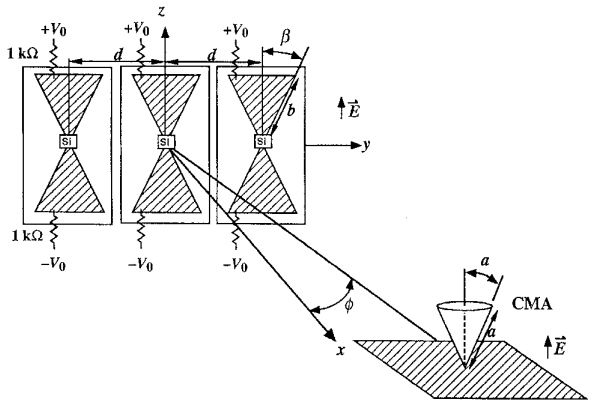

Fig. 2. Schematic diagram of experimental setup showing spatial relationship between three bowtie antennas and short conical monopole antenna (CMA) field probe. Arrival time of optical pulses at two leftmost antennas controlled by optical true time delay, as described in text. CMA distance from antenna plane is 1 m.

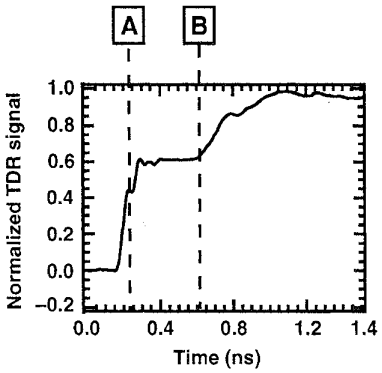

Fig. 3. Reflected voltage from time domain reflectometry (TDR) measurement. Marker A: Bow-tie antenna feed-point (apex). Marker B: Bow-tie antenna truncation.

III. Results

A. Single Element

The normalized reflected-voltage TDR signal from the bow-tie antenna is shown in Fig. 3. To the left of Marker A, the excitation pulse is propagating without reflection in the $Z_0 = 50\,\Omega$ feed line. When the pulse meets the antenna feed point (Marker A), it is partially reflected and partially transmitted because of the impedance mismatch between the $Z_0 = 50\,\Omega$ feed line and the higher impedance of the bow-tie antenna. Between the feed point (Marker A) and the bow-tie antenna truncation (Marker B) there is no additional reflection, indicating a constant characteristic impedance, Z_A. We calculate that $Z_A = 220\,\Omega$ which gives the 63% reflection coefficient that is observed.

The transmission-line behavior is in agreement with the measurements of Rutledge and Muha [18], who concluded that the terminal impedance of an electrically long bow-tie antenna could be calculated from the static capacitance and inductance of the antenna. This behavior is also similar to the transmission-line behavior described by Krauss [19] for a

similar three-dimensional analog, the biconical antenna. Thus, the characteristic impedance of the bow-tie antenna (in free space) can be found from the transmission-line formula

$$Z_A = \sqrt{\frac{\mu_o}{\varepsilon_o}} \cdot \frac{K(k)}{K'(k)} \tag{1}$$

where $k = \tan^2[(\pi/4) - (\beta/2)]$ and K and K' are elliptic integrals. The calculated value for our antenna is $Z_A = 254\,\Omega$, which is somewhat larger than our measured value ($Z_A = 220\,\Omega$). This may be partially due to the effect of the thin dielectric substrate, which gives a slightly larger value for the effective permittivity.

At Marker B we notice a reflection with a slow risetime. We modeled this as arising from a complex load impedance, Z_L, presented by free space at the truncation. The slow risetime indicates that the load contains a capacitive reactance, while the lack of an abrupt step indicates that the real part of the load (the radiation resistance), R_{rad}, is matched to the antenna impedance, (i.e., $R_{rad} = Z_A$). The capacitive reactance of Z_L is small at short wavelengths; hence, the short-wavelength input impedance of the bow-tie antenna will approach the characteristic impedance as expected. On the other hand, when the bow-tie antenna is electrically short (at very long wavelengths) the capacitive reactance of Z_L dominates and the bow-tie antenna's terminal impedance will be primarily a capacitive reactance, as expected.

Based on these measurements, we developed a simple transmission-line model in order to describe the salient features of energy storage and to provide an easily calculated figure of merit for the optimization of design parameters. The transmission-line model for an individual laser-triggered UWB bowtie antenna element is shown in Fig. 4(a). The location $s = 0$ corresponds to the antenna apex (i.e., the position of the photoconductor), and $s = b$ corresponds to the truncation. Note that the radiation resistance, which is equal to the antenna characteristic impedance $[Z_A(\beta) = R_{rad}(\beta)]$, is also a function of the angle β. In the model, the photoconductor is assumed to have a very large nontriggered (open-state) resistance ($\gg Z_A$) and a finite resistance of R_{SW} when triggered (closed). There also exists a parasitic capacitance, C_{SW} that reduces the effective risetime of the pulse produced when the photoconductor is triggered. For added simplicity, we have shown the model as unbalanced (i.e., one side of the transmission line is grounded), and we have neglected nonradiative or loss resistance.

While the photoconductor is in its nontriggered state, the transmission line is charged to the voltage $2V_0$. In the steady state ($t < 0$), two counter-propagating traveling waves exist, both with equal amplitude. As shown in Fig. 4(b), $V_+ = V_- = V_0$.

Now, let us assume the ideal case of a negligible parasitic capacitance, C_{SW}. When the photoconductor is triggered, the sudden temporal change in transmission-line boundary conditions causes a change in the traveling wave amplitudes. Before the photoconductor is triggered, the initial voltage reflection coefficient at $s = 0$, $t < 0$, is $\rho_{off} = 1$. After triggering, $t \geq 0$, the new voltage reflection coefficient

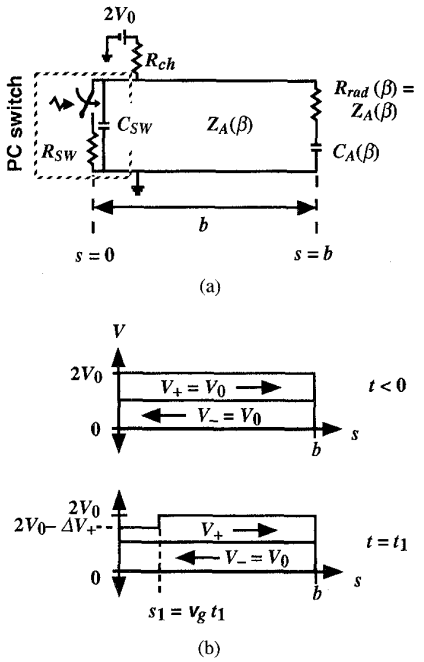

Fig. 4. (a) Transmission-line (TL) model of a single photoconductive (PC) switch driven array element and (b) traveling waves on TL while switch is open ($t < 0$) and just after switch has closed ($t = t_1$).

becomes

$$\rho_{on} = \frac{R_{SW} - Z_A}{R_{SW} + Z_A}. \tag{2}$$

Thus, the amplitude of the right-propagating wave, V_+, changes. The change in amplitude of this wave, ΔV_+, is determined by the change in reflection coefficient that occurs at $s = 0$, $t = 0$, as given by

$$\begin{aligned} \Delta V_+ &= V_0 \cdot (\rho_{off} - \rho_{on}) \\ &= 2V_0 \cdot \frac{Z_A}{R_{sw} + Z_A}. \end{aligned} \tag{3}$$

At $t = t_1$, shortly after the switch is triggered to the on-state, ΔV_+ has traveled to $s = s_1 = v_g t_1$ where v_g is the group velocity in the antenna as illustrated in Fig. 4(b). When the step, ΔV_+, reaches $s = b$, its rising edge is delivered to the matched radiation resistance with a peak power given by

$$\begin{aligned} P_{Pk} &= \frac{\Delta V_+^2}{Z_A} \\ &= 4V_0^2 \cdot \frac{Z_A}{(R_{sw} + Z_A)^2}. \end{aligned} \tag{4}$$

We can use P_{pk} as a figure of merit in evaluating the expected performance of a single element. Given that the value of R_{SW} is predetermined by the available laser energy, we can realize the highest peak power by adjusting the antenna angle, β, to achieve the optimum value of Z_A. As expected, the maximum peak power occurs when $Z_A = R_{SW}$. Note that by using the antenna itself for energy storage, we are not constrained by the necessity to match the antenna impedance to a particular feed-line impedance.

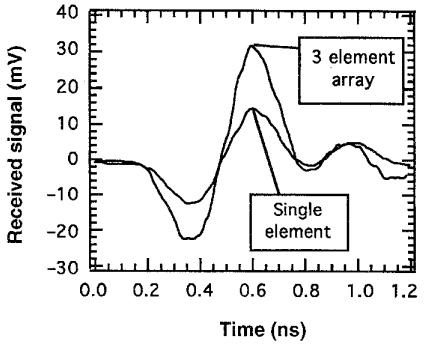

Fig. 5. Received waveforms at azimuth angle of $\phi = 30°$ and relative trigger delay of $T = 160$ ps between adjacent elements. Optical trigger blocked to all but one of bowtie antenna elements (single element) and all three antennas activated (array).

Before characterizing an N-element array we measured the pattern of a single laser-triggered antenna element. The signal radiated by a single element of the $N = 3$ element array and received by a CMA field probe at $\phi = 30°$ is shown in Fig. 5 (single element). The amplitude and shape of the signal received by the CMA field probe was found to be almost independent of the azimuth angle, ϕ. A longer antenna would be required to realize a nonisotropic azimuthal pattern.

The temporal shape of the radiated field arises from taking the first time derivative of the step-like excitation and an additional time derivative for low frequencies where the transmitting antenna is short [20]. A short receiving antenna (such as our CMA) adds one more time derivative to the received waveform. Since our excitation pulse contains a wide spectrum of frequencies, the transmitting antenna can be classified as electrically short over only a fraction of the pulse spectrum. Hence, the received signal of Fig. 5 is intermediate between the shape of a second time derivative and a third time derivative of the step-like excitation pulse.

B. N-Element Array

Next, the array of three elements was characterized. Fig. 6(a) shows the received signal from the three-element array with 0-ps optical trigger delay between elements. The evolution of the received signal is shown as we scan the azimuth angle of the receiving antenna (as shown in Fig. 2) from $\phi = 0°$ to $\phi = 80°$. The received pulse shape is best understood if one considers the operation of the array in the time domain. At a far-field observation point, the relative time it takes for a radiated pulse to travel from each of the individual elements to an observer in the far-field is dependent on ϕ. Since the observed field is the linear superposition of the fields radiated by each of the individual elements, the received signal's shape and amplitude are also dependent on ϕ. The largest amplitude signal is observed when the pulses from each of the $N = 3$ radiators arrive simultaneously. The difference in the far field arrival time, Δt, of the independent pulses that were simultaneously triggered in adjacent neighbors in the array is given by

$$\Delta t = \left(\frac{d}{c}\right) \sin \phi \tag{5}$$

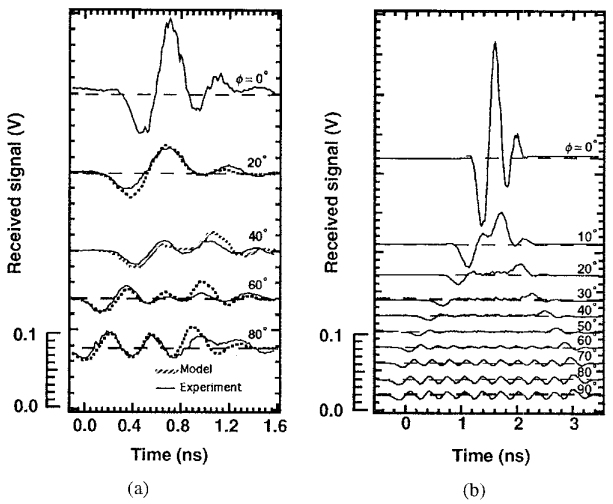

Fig. 6. (a) Received waveform as a function of azimuth angle, ϕ, for three-element array with all elements triggered simultaneously. Computer model results are shown for $\phi > 0$ as described in the text and (b) computer model of received signal from $N = 10$ element array assuming same optical trigger energy per element as in (a).

where c is the free-space velocity of light. When $\phi = 0°$ (or 180°) all three pulses overlap perfectly and the temporal shape of the received signal is identical to that of the pulse radiated by a single element; but, as ϕ is increased, the pulse arrival time varies significantly between elements, causing the received signal to broaden and decrease in amplitude. In the frequency domain, the broad pulse that appears in the sidelobes can be viewed as arising from low-frequency components that do not experience destructive interference in this closely spaced array.

In order to demonstrate that the received pulse could be determined by a superposition of the pulses radiated by each of the individual antennas, we developed a semi-empirical computer model. The model takes the experimentally observed single-element signal that was received at $\phi = 0°$, scales it by $1/N$, and stores it. This represents the pulse radiated by a single element. By numerical addition of the N single-element pulses with the correct inter-element time delay as determined by (5), the expected received signal can be determined as a function of the following parameters: N, ϕ, and d. The model was verified on the $N = 3$, $d = 10$ cm experimental results, as shown in Fig. 6(a). The signal received at $\phi = 0°$ was used to determine the single-element pulse shape and to numerically calculate the response at other angles.

Differences between the model and experiment arise from a number of causes. First, the pulse *amplitude* radiated by each of the elements is not quite identical. Second, the measurements were not completed in an anechoic chamber, and metallic objects (such as a nearby optical laboratory table) were close enough that small spurious reflections could occur within the time window of the measurement. RF absorbing foam was placed on the metal table to help control reflections, but the foam's effectiveness is limited at frequencies below approximately 1 GHz. Finally, some time-delayed spurious reflections from neighboring antenna elements can also occur within the time window of the measurement.

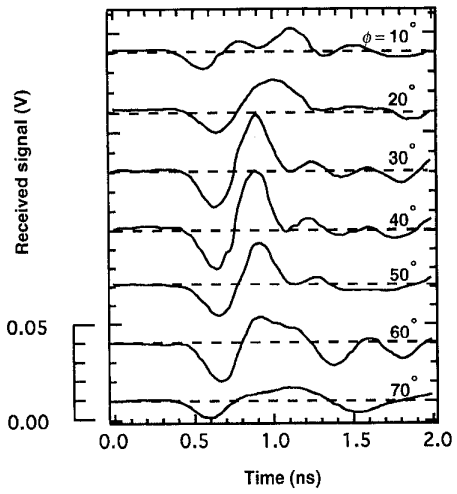

Fig. 7. Received signal at various azimuth angles, ϕ, with relative optical trigger delay of T = 160 ps between adjacent antenna elements.

The empirical computer model was also used to model larger element arrays. The result for an N =10 elements, d = 10 cm array is shown in Fig. 6(b). Comparing this with the N = 3 result, we note that the received peak voltage scales as N, implying that the received peak power scales as N^2.

We can also adjust the array to point in directions other than $\phi = 0°$. For a given angle, we can adjust the relative triggering time of each of the bowtie elements so that the pulse from each of the three elements arrives simultaneously for observers at that angle, producing the highest peak power at that angle. We tested this by implementing a 160-ps true time delay of the optical trigger pulse between adjacent elements in our three element array. The fields from each of the elements should add together in free space at $\phi = 30°$ to produce a signal at the field probe three times as large and, hence, a received peak power nine times as large.

In the actual experiment (Fig. 5), the charge voltage, V_0, dropped slightly when additional elements were added because of the high output impedance of the pulsed power supply; hence the peak received signal scaled by a factor of 2.3 over that obtained by a single element rather than scaling by a factor of 3. As shown in Fig. 7, as we move away from $\phi = 30°$, the received pulse broadens and decreases in amplitude as the pulses from the three elements no longer arrive simultaneously.

In Fig. 8, we plot the normalized peak power received versus angle, ϕ, for the case of no delay between elements and for the case with a delay of 160 ps between adjacent elements. With a 0-ps true time delay between elements, we note that the beam points toward 0° (broadside). Although the theoretical pointing angle for the 160-ps delay is 29°, we measure the largest peak field at 40° with measurements made in 10° increments. We note that exact calibration of the 0° pointing angle was difficult because of spurious reflections from nearby optical tables; thus the pattern may be subject to some skew. In the future, we plan to repeat measurements in an anechoic chamber. The solid lines in Fig. 8 show the shape of the pattern predicted by the quasiempirical linear superposition model described above.

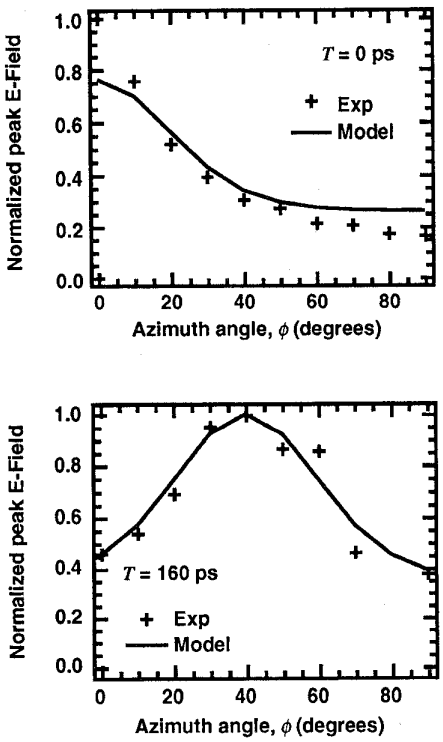

Fig. 8. Peak power versus azimuth angle, ϕ, with T = 160 ps and T = 0 ps optical trigger delay, respectively, between adjacent antenna elements. Note UWB beam steering.

IV. Conclusion

The beam-forming and beam-steering capabilities that were demonstrated rely on the ability to coherently add UWB radiation from each element of an array of UWB antennas. For UWB signals, the coherence requirement can be understood in terms of the ability of each radiator to radiate an identical pulse with negligible jitter between elements. Hence, the far fields consist of a time-domain superposition of the pulses radiated by each of the individual elements. While a three-element system was used here, this technique is equally applicable to an N-element array with the peak power received by an antenna in the far-field scaling as N^2 due to the coherent addition of electric fields.

We have verified that such a linear superposition model produces a good prediction of the received signal. In the experimental setup we used photoconductors triggered by a mode-locked laser pulse train to produce the jitter-free synchronization that was necessary for UWB beam-forming. Furthermore, our experiment showed how optical true time delay could be used to steer a UWB beam.

The success of this approach suggests the possibility of a very practical UWB optically controlled phased-array antenna system. There are a variety of advantages to using an instantaneously UWB signal, including the ability to realize a practical spread-spectrum communications system by introducing time-hopping onto the laser pulse train. Such a time-hopped pulse train would be very difficult to intercept because it would be spread in both the time and frequency domains.

In this first demonstration, the photoconductor was used as a passive fast-closing switch driving a UWB antenna. We developed a transmission-line energy storage model for our configuration of a closing switch driving a bow-tie antenna. The model illustrates how the features of energy storage, UWB pulse generation, and radiation are combined into one unit. Clearly this passive approach has a limited efficiency. However, we are now building an active array using wide-band monolithic microwave integrated circuit (MMIC) amplifiers driving UWB antennas. UWB pulse generation can be triggered in the MMIC amplifiers [21] by a small impulse excitation from a laser-pulse-triggered photoconductor or fast photodiode. Furthermore, this approach will allow integration of optoelectronic attenuators for amplitude tapering [22]. With this approach, there will be enough laser energy available to trigger over 100 MMIC/antenna elements with a single compact diode-pumped laser.

ACKNOWLEDGMENT

The authors would like to acknowledge S. E. Saddow and L. J. Jasper, Jr. for their relevant discussions of this work, and Y. S. Lai for fabricating the field probe antenna.

REFERENCES

[1] W. Ng, A. A. Walston, G. L. Tangonan, J. J. Lee, I. L. Newberg, and N. Bernstein, "The first demonstration of an optically steered microwave phased array antenna using true-time delay," *IEEE J. Lightwave Technol.*, vol. 9, pp. 1124–1131, 1991.

[2] H. Zmuda and E. N. Toughlian, Eds., *Photonic Aspects of Modern Radar.* Boston: Artech House, 1994.

[3] N. A. Riza, "Liquid crystal-based optical time delay units for phased array antennas," *J. Lightwave Technol.*, vol. 10, pp. 1974–1984, 1994.

[4] E. H. Monsay, K. C. Baldwin, and M. J. Caccuitto, "Photonic true time delay for high-frequency phased array systems," *IEEE Photonics Technol. Lett.*, vol. 6, pp. 118–120, Jan. 1994.

[5] W. D. Jemison and P. R. Herczfeld, "Acousto-optically controlled true time delays," *IEEE Microwave Guided Wave Lett.*, vol. MTT-3, pp. 72–74, 1993.

[6] R. C. Dixon, *Spread Spectrum Systems.* New York: Wiley, 1984.

[7] E. E. Funk, S. E. Saddow, and L. J. Jasper Jr., "Optically controlled spread-spectrum RF data link," in *1996 MTT-S Symp.*, Paper TH3D-5, 1996.

[8] C. H. Lee, "Picosecond optics and microwave technology," *IEEE Trans. Microwave Theory Tech.*, vol. 38, no. 5, pp. 596–607, 1990.

[9] J. T. Darrow, B. B. Hu, X.-C. Zhang, and D. H. Auston, "Subpicosecond electromagnetic pulses from large-aperture photoconducting antennas," *Opt. Lett.*, vol. 15, pp. 323–325, 1990.

[10] G. H. Brown and O. M. Woodward, Jr., "Experimentally determined radiation characteristics of conical and triangular antennas," *RCA Rev.*, vol. 13, pp. 425–452, Dec. 1952.

[11] A. Kim, R. J. Youmans, R. Zeto, M. Weiner, J. Fishback, J. Tsinetakes, and B. Lalevic, "Photoconductive impulse generation and radiation," *IEEE Trans. Microwave Theory Tech.*, vol. 39, pp. 2026–2030, 1991.

[12] N. M. Froberg, B. B. Hu, X. C. Zhang, and D. H. Auston, "Terahertz radiation from a photoconducting antenna array," *IEEE J. Quantum Electron.*, vol. 28, pp. 2291–2301, 1992.

[13] A. S. Welling, B. B. Hu, N. M. Froberg, and D. H. Auston, "Generation of tunable narrow-band THz radiation from large aperture photoconducting antennas," *Appl. Phys. Lett.*, vol. 64, pp. 137–139, 1994.

[14] G. Arjavalingam, Y. Pastol, J.-M. Halbout, and G. V. Kopcsay, "Broadband microwave measurements with transient radiation from opto-electronically pulsed antennas," *IEEE Trans. Microwave Theory Tech.*, vol. 38, pp. 615–621, 1990.

[15] Y. Pastol, G. Arjavalingam, J.-M. Halbout, and G. V. Kopcsay, "Coherent broadband microwave spectroscopy using picosecond opto-electronic antennas," *Appl. Phys. Lett.*, vol. 54, pp. 307–309, 1989.

[16] R. Lawton, S. Riad, and J. Andrews, "Pulse and time-domain measurements," *Proc. IEEE,* vol. 74, pp. 77–81, 1986.

[17] C. W. Harrison, Jr., and C. S. Williams, Jr., "Transients in wide-angle conical antennas," *IEEE Trans. Antennas Propagat.*, vol. AP-13, pp. 236–246, 1965.

[18] D. B. Rutledge and M. S. Muha, "Imaging antenna arrays," *IEEE Trans. Antennas Propagat.*, vol. AP-30, pp. 535–540, 1982.

[19] J. D. Kraus, *Antennas.* New York: McGraw-Hill, 1988, ch. 2.

[20] R. W. Ziolkowski, "Properties of electromagnetic beams generated by ultra-wide bandwidth pulse-driven arrays," *IEEE Trans. Antennas Propagat.*, vol. AP-40, pp. 888–904, 1992.

[21] S.-L. L. Huang, C. H. Lee, and H. L. A. Hung, "Optically controlled generation and true-time-delay phase shifts of broad-band 60 GHz signals," *IEEE Microwave Guided Wave Lett.*, vol. 3, pp. 42–44, 1993.

[22] S. E. Saddow and C. H. Lee, "Optical control of microwave-integrated circuits using high-speed GaAs and Si photoconductive switches," *IEEE Trans. Microwave Theory Tech.*, vol. 43, pp. 2414–2420, 1995.

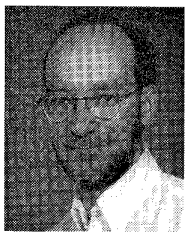

Eric E. Funk received the B.S. degree in physics from Rensselaer Polytechnic Institute, Troy, NY, in 1988. He received the M.S. and Ph.D. degrees in electrical engineering from University of Maryland, College Park, MD, in 1991 and 1995, respectively.

From 1989 to 1995, he was a Graduate Research Assistant at the University of Maryland with a research interest in photoconductivity. In 1995, he became a Postdoctoral Researcher working at the U.S. Army Research Laboratory, Adelphi, MD. His present research interest is in opto-electronic ultra-wideband systems.

Chi H. Lee for a photograph and biography, see p. 1289 of the June 1995 issue of this TRANSACTIONS.